Mesostructured Iron Oxyhydroxides. 1. Synthesis, Local Structure, and Magnetism

G. Wirnsberger,*[,†] K. Gatterer,[‡] H. P. Fritzer,[‡] W. Grogger,[§] B. Pillep,[||,⊥] P. Behrens,*[,||] M. F. Hansen,[#] and C. Bender Koch*[,▽]

Institut für Anorganische Chemie, Karl-Franzens-Universität Graz, Schubertstr. 1, A-8010 Graz, Austria, Institut für Physikalische und Theoretische Chemie, Technische Universität Graz, Rechbauerstr. 12, A-8010 Graz, Austria, Forschungsinstitut für Elektronenmikroskopie und Feinstrukturforschung, Technische Universität Graz, Steyrergasse 17, A-8010 Graz, Austria, Institut für Anorganische Chemie, Universität Hannover, Callinstr. 9, D-30167 Hannover, Germany, Rechtsanwaltskanzlei Kador und Partner, Corneliusstrasse 15, D-80469 München, Germany, Department of Physics, Building 307, Technical University of Denmark, DK-2800 Lyngby, Denmark, and Chemistry Department, The Royal Veterinary and Agricultural University, Thorvaldsenvej 46, DK-1871 Frederiksberg C, Denmark

Received February 18, 2000. Revised Manuscript Received July 26, 2000

The synthesis, local structure, and magnetism of lamellar iron(III) oxyhydroxide−surfactant composites prepared by two different methods have been investigated in detail. In the first method, Fe(II) solutions are oxidized by H_2O_2 in the presence of $C_nH_{2n+1}OSO_3^-Na^+$ surfactants (n = 10, 12, 14, 16, 18), leading to lamellar composites with an inorganic wall thickness of around 28 Å. When a second method is used, namely, aging an Fe(III) solution for selected times after slightly increasing the pH with NH_3 and subsequent addition of the surfactant, the inorganic wall thickness can be tuned between 19 and 26 Å, employing the same surfactants. EXAFS analysis of the Fe K edge X-ray absorption spectra reveals that the local structure of the inorganic part is a reminder of those found for the bulk iron oxyhydroxides goethite and akaganéite; that is, $[Fe(O,OH)_6]$ octahedra are predominantly connected by common edges and corners, the ratio of edge to corner sharing being similar to the mentioned bulk oxyhydroxides. Whereas coordination numbers for the first oxygen coordination shell are around 6, confirming an octahedral (or distorted octahedral) coordination around the Fe ions, coordination numbers found for the second and third Fe···Fe neighbors are low (around 2), indicating the presence of a considerable amount of vacancies around the central absorber ion or, as an alternative description, a low degree of condensation of the oxyhydroxide. Complementary to the local structural picture given by EXAFS, Mössbauer spectra elucidate the inorganic iron oxyhydroxide walls to be built up by domains of different crystallinity. The crystallinity is sensitive to the synthesis conditions used in the preparation. For example, under aging in the presence of NH_3, longer aging times and higher temperatures result in a larger overall crystallinity of the inorganic part. By carefully controlling the reaction parameters, the thickness of the inorganic layers can be varied from around 19 Å to around 30 Å; also, the blocking temperatures of these superparamagnetic compounds observed by zero-field-cooled magnetization measurements can be controlled in the range between 4 and 30 K.

Introduction

A focus in contemporary solid state chemistry and physics is taken on the preparation and investigation of size-confined materials in the nanometer-size range. The interest in these materials arises because optical, electronic, and magnetic properties of materials change dramatically when the particle size is reduced to a critical limit. In the size regime between single molecules and bulk materials, various chemical methods have been shown to be suitable tools to achieve a size confinement. This holds also for iron oxides and iron oxyhydroxides, which in their bulk forms find applications, for example, as pigments and catalysts.[1] Nanostructured iron oxides are also of interest for applications, for example, in magnetic storage media.[2] From a

* To whom correspondence should be addressed. E-mails: gernot.wirnsberger@kfunigraz.ac.at; Peter.Behrens@mbox.acb.uni-hannover.de; Chr.Bender.Koch@kemi.kvl.dk.
† Karl-Franzens-Universität Graz.
‡ Institut für Physikalische und Theoretische Chemie, Technische Universität Graz.
§ Forschungsinstitut für Elektronenmikroskopie und Feinstrukturforschung, Technische Universität Graz.
|| Universität Hannover.
⊥ Rechtsanwaltskanzlei Kador und Partner.
Technical University of Denmark.
▽ The Royal Veterinary and Agricultural University.

(1) Cornell, R.; Schwertmann, U. *The Iron Oxides*; VCH: Weinheim, 1996.
(2) Leslie-Pelecky, D. L.; Rieke, R. D. *Chem. Mater.* **1996**, *8*, 1770.

10.1021/cm991211+ CCC: $20.00
Published on Web 04/18/2001

chemical perspective, different approaches can be used to limit the size of iron oxide particles. Amorphous[3] or crystalline silica matrixes[4,5] can be used to limit the growth of the particles resulting in isolated iron oxide/oxyhydroxide units. Other stable matrixes can in principle also be used, and successful stabilization of size-limited iron oxides/oxyhydroxides was reported in vesicles,[6,7] resins,[8] microemulsions,[9] Langmuir−Blodgett films,[10] and polymers.[11−13]

Another synthetic strategy uses self-assembly of inorganic precursors with organic surfactants. This was first reported for SiO_2−surfactant composites.[14,15] These mesostructured composites possess periodicities between ≈20 and 200 Å. The thickness of the inorganic parts varies in the range from ∼10 to 40 Å. The surfactant headgroup can be varied, allowing one to actively control the interaction between the inorganic precursors and the surfactants. A cooperative self-assembly mechanism has been proposed for the formation of these composites.[16] On its basis, a variety of non-silica-based mesostructured materials have been produced.[17] For iron oxides/oxyhydroxides as the inorganic part of the final composite, surfactants carrying sulfate headgroups were successfully employed in the synthesis of composites with limited size dimensions of the iron oxide/oxyhydroxide constituents of the inorganic part.[18] These composites have been reported to be lamellar; that is, they are comprised of sequential surfactant layers and iron oxide/oxyhydroxide layers. They were prepared by oxidizing Fe^{2+}-containing solutions with H_2O_2 in the presence of $C_nH_{2n+1}OSO_3^-$ surfactants. Most importantly, the thickness of the inorganic layers could be adjusted to around 16 Å or to around 11 Å by using short (n = 10, 12, 14) or long (n = 16, 18) alkyl chain surfactants, respectively. The superparamagnetic blocking temperature of these composites observed by zero-field-cooled (ZFC) magnetization measurements could be tuned by adjusting the inorganic wall thickness (16 and 3 K for the composites with 16- and 11-Å-thick inorganic walls, respectively).

In a preliminary communication we reported two alternative synthetic routes to such composites by employing the same surfactants; both our methods start from Fe^{3+}-containing solutions and make use of the hydrolytic chemistry of Fe^{3+} in weakly acidic media (pH around 2).[19] By these synthetic methods, it is possible to extend the size of the inorganic part up to around 26 Å. As we will show here, this also results in a change of the (superpara)magnetic properties. In this article we present a detailed study of the synthesis, the local structure, and magnetism of such composites. The main focus is on the active use of the hydrolysis chemistry of Fe(III)—initiated by H_2O_2 or NH_3 addition—for tuning the structural and magnetic properties of these composites. In addition, on the basis of the present observations, we propose a reaction mechanism for the different syntheses routes to such composites. In a follow-up paper we focus on the soft chemical restructuring of samples made in Fe^{3+}/surfactant solutions *without* the addition of auxiliary reagents.

Experimental Section

Sample Preparation. The first method is similar to the one reported by Tolbert et al.[18] Ten milliliters of a 0.07 mol L^{-1} $C_nH_{2n+1}OSO_3^-$−Na^+ solution (in the following denoted as Cn and supplied by Aldrich in the case of C12 and Henkel in the other cases, respectively) is added to 50 mL of a 0.1 mol L^{-1} $FeCl_2$ solution. Fe(II) and surfactant solutions were warmed to 318, 325, and 335 K before mixing for the composites of C14, C16, and C18, respectively. The heating was necessary because of the lower solubility of the longer alkyl chain surfactants at room temperature. Thereafter, 10 mL of a 3 wt % H_2O_2 solution was dropped into these clear solutions under vigorous stirring (around 400 rpm) within 150 s. It is worth pointing out that—in contrast to the synthesis by Tolbert el al.[18]—the solutions were clear when H_2O_2 was added (when the initial Fe(II)/surfactant solution is allowed to react for several minutes, a crystalline Fe(II)−surfactant compound is obtained, which then can also be transformed into an Fe(III)−surfactant composite by oxidation[18]). The synthesis mixtures were then held at the corresponding synthesis temperatures for 30 min and stirred during this time. The mixtures changed their color from slightly green to orange-brown after the H_2O_2 addition (indicating oxidation and hydrolysis). Finally, the reaction products were washed with 200 mL of deionized H_2O. In the following, we refer to compounds made by this route as Cn/H_2O_2.

The second method starts from $FeCl_3$. Generally, 5 mmol of $FeCl_3 \cdot 6H_2O$ was dissolved in 50 mL of deionized H_2O. Afterward, 2, 5, 8, or 11 mL of a 2.5 wt % NH_3 solution was dropped slowly into the Fe(III) solution under vigorous stirring. After being stirred for 2 h, the solutions were optically transparent but had changed their colors from orange to deep red, indicative of condensed polymeric Fe(III) species. The pH values of the precursor solutions 2 h after the addition of 2, 5, 8, or 11 mL of NH_3 were measured to be 1.85, 1.90, 2.00, and 2.13, respectively. In a final step—after exactly 120 min—10 mL of a 0.07 mol L^{-1} surfactant solution was mixed with the precursor solutions. Again, the synthesis temperatures for composites with longer alkyl chains were 318, 325, and 335 K, respectively. Reaction mixtures were stirred for an additional 30 min at the adjusted reaction temperature. The remaining steps were the same as those for the preparations with H_2O_2. We refer to compounds made by this route as Cn/

(3) Chanéac, C.; Tronc, E.; Jolivet, J. P. *J. Mater. Chem.* **1996**, *6*, 1905.
(4) Abe, T.; Tachibana, Y.; Uematsu, T.; Iwamoto, M. *Chem. Commun.* **1995**, 1617.
(5) Fröba, M.; Köhn, R.; Bouffaud, G.; Richard, O.; van Tendeloo, G. *Chem. Mater.* **1999**, *11*, 2858.
(6) Mann, S.; Hannington, J. P. *J. Colloid Interface Sci.* **1988**, *122*, 326.
(7) Yaacob, I. I.; Nunes, A. C.; Bose, A. *J. Colloid Interface Sci.* **1995**, *171*, 73.
(8) Ziolo, R. F.; Gianelis, E. M.; Weinstein, B. A.; O'Horo M. P.; Ganguly, B. N.; Mehrotra, V.; Russell, M. W.; Huffmann, D. R. *Science* **1992**, *257*, 219.
(9) López-Quintela, M.-A.; Rivas, J. *J. Colloid Interface Sci.* **1993**, *158*, 446.
(10) Sohn, B. H.; Cohen, R. E. *Chem. Mater.* **1997**, *9*, 264.
(11) Kommareddi, N. S.; Tata M.; John, V. T.; McPherson, G. L.; Herman M. F.; Lee, Y.-S.; O'Connor, C. J.; Akkara, J. A.; Kaplan, D. L. *Chem. Mater.* **1996**, *8*, 801.
(12) Breulmann, M.; Cölfen, H.; Hentze, H.-P.; Antonietti, M.; Walsh, D.; Mann, S. *Adv. Mater.* **1998**, *10*, 237.
(13) Butterworth, M. D.; Armes, S. P.; Simpson, A. W. *Chem. Commun.* **1994**, 2129.
(14) Kresge, C. T.; Leonowicz, M. E.; Roth, W. J.; Vartuli, J. C.; Beck, J. S. *Nature* **1992**, *359*, 710.
(15) Beck, J. S.; Vartuli, J. C.; Roth, W. J.; Leonowicz, M. E.; Kresge, C. T.; Schmitt, K. D.; Chu, C. T. W.; Olson, D. H.; Sheppard, E. W.; McCullen, S. B.; Higgins, J. B.; Schlenker, J. L. *J. Am. Chem. Soc.* **1992**, *114*, 10834.
(16) Huo, Q.; Margolese, D. I.; Ciesla, U.; Feng, P.; Gier, T. E.; Sieger, P.; Leon, R.; Petroff, P. M.; Schüth, F.; Stucky, G. D. *Nature* **1994**, *368*, 317.
(17) For summaries on non-silica-based mesostructured materials see: Behrens, P. *Angew. Chem., Int. Ed. Engl.* **1996**, *35*, 515; Sayari, A.; Liu, P. *Mesoporous Mater.* **1997**, *12*, 149.
(18) Tolbert, S. H.; Sieger, P.; Stucky, G. D.; Aubin, S. M. J.; Wu, C.-C.; Hendrickson, D. N. *J. Am. Chem. Soc.* **1997**, *119*, 8652.
(19) Wirnsberger, G.; Gatterer, K.; Behrens, P. *J. Mater. Chem.* **1998**, *8*, 1509.

NH_3. To investigate the effect of the aging times on the thickness of the inorganic part of the layered composites, precursor solutions were in addition aged for various times, starting from 50 min up to 1500 min.

Characterization. *X-ray Diffraction.* Powder X-ray diffraction (XRD) patterns were obtained in Bragg−Brentano geometry (Cu Kα radiation) on a Philips PW 1710 diffractometer equipped with a graphite secondary monochromator. Slits were fixed to 0.25° or 0.5° for the entrance and to 1.0° for the outgoing beam. Additional experiments were performed with Cr Kα radiation to check for possible transformations during XRD data collection with Cu Kα radiation, which is strongly absorbed by Fe.

Elemental Analysis. Carbon, hydrogen, nitrogen, and sulfur contents of mesolamellar composites were determined by the use of an automatically working analyzer EA 1108 CNSO-O (Carlo Erba). Samples occluded in a stannic foil were heated to 1293 K within 2 s and the evolved gases were analyzed by a conventional gas-phase chromatograph. Sulfonamide served as a calibration standard and empty tin cups were utilized for blank experiments. To derive information about the iron/surfactant ratios, typically about 5 mg of a sample was combusted in an oven at 1173 K under an oxygen atmosphere and the mass of the residue was determined.

Electron Microscopy. Transmission electron micrographs (TEM) were taken on a Philips EM 420 operating at 120 kV and on a Philips CM 20 operating at 200 kV. For this purpose, samples were dusted on a Cu grid. For scanning electron microscopy (SEM), a Leitz ARM 1000 was employed. Samples for SEM were sputtered with a thin Au film.

X-ray Absorption Spectroscopy. X-ray absorption fine structure (XAFS) measurements at the Fe K edge (77 K) were performed at the Hamburg synchrotron laboratory (HASYLAB) at stations A1 and E4 (DESY), using the radiation from the storage ring DORIS III operating at 4.432 GeV (injection current of 100 mA). A Si(311) double monochromator was used for the monochromatization of the radiation; the first crystal of the double-crystal monochromator was detuned to 50% to minimize the contribution of higher harmonics. The energy resolution was around 1 eV at 7.7 keV. Samples suited for XAFS were prepared by pressing around 20−60 mg of the compound to be investigated with polyethylene into a disk; the exact amount of each sample was selected to give edge jumps in $\Delta\mu d$ of 0.5−1. Data analysis of spectra recorded at 77 K was performed with the program WINXAS97[20] in the following way: Spectra were first energy calibrated by setting the maximum of a simultaneously measured Eu_2O_3 L_2 edge to 7.6620 keV. The first inflection point of the Fe K edge of metallic Fe then occurs at 7.1120 keV. For underground correction, a Victoreen fit was adjusted to the pre-edge region, extrapolated to the region above the edge and subtracted. Thereafter, the absorption at high energies was normalized to 1.0 and E_0 determined (first inflection point of the edge). For EXAFS analysis, spectra were converted into *k*-space and EXAFS oscillations were extracted by using a cubic-spline μ_0 fit weighted with $k = 3$ in the wave vector range $k = 2-16$ Å^{-1}. $\chi(k)k^3$ functions obtained in this way were Fourier transformed applying a Bessel window function. The first peaks of the Fourier transform (FT), which correspond to the oxygen shells, were back-transformed in the range $R = 1.2-2.0$ Å; the peaks of the second and third shells corresponding to Fe···Fe distances were back-transformed together ($R = 2.3-3.4$ Å). Finally, the desired parameters (e.g., bond distances) were derived by weighing the resulting functions with $k = 3$ (back-transform of the first peak) and $k = 2$ (second and third peak) and fitting them with phase and amplitude functions calculated with FEFF 7.02.[21−23]

Magnetic Measurements. For the characterization of the magnetic behavior of the composites, an ac-susceptometer/dc-magnetometer from Lakeshore Co. (model 7221) was employed. For ZFC dc measurements, samples held in Delrin cups were cooled to 4.5 K in a zero applied field and adjusted in position to give a maximal signal. Thereafter, the sample was demagnetized to ensure that no residual effects due to the adjusting field remained. After this, a constant field of typically 200 kA m^{-1} was switched on and signals were recorded in steps of 1 K up to 20 K and in steps of 5 K from 20 K above the peak maximum up to the final temperature. After this measurement, the field was maintained and the sample was again cooled to 4.5 K and then measured up to the final temperature. For a series of ac measurements, the frequency of the oscillating field (constant for a series) was varied from 5 to 1000 Hz. Generally, low fields (e.g., 1100 A m^{-1}) were applied (without additional dc fields). Phase shifts and sample geometry were corrected with an in-house program.

Mössbauer Measurements. Mössbauer spectra were measured in several steps between 17 and 293 K in zero applied fields and at 80 K in a field of 0.8 T applied perpendicular to the direction of the γ-rays. The temperature accuracy was 0.5 K at 17 and 1 K at higher temperatures. All measurements were done using the same absorber in the whole temperature range, which causes high absorption at intermediate and high temperatures; some spectra may therefore be subject to saturation effects. However, the conclusions drawn are not affected by these effects. Mössbauer parameters were estimated, because of a lack of suitable models resulting from the structural complexity of the inorganic part, corresponding to the peak positions. All isomer shifts are given with respect to that of α-Fe at room temperature.

Results and Discussion

Tuning the Inorganic Wall Thickness. The oxidation of an Fe(II) solution with H_2O_2 in the presence of C*n* leads to the immediate precipitation of mesolamellar composites. The corresponding XRD patterns exhibit only d_{001} reflections and no indication of the presence of other symmetries, for example, cubic or hexagonal, is found. Typical XRD patterns for a surfactant series with increasing alkyl chain length are shown in Figure 1. When the d_{001} spacing (Table 1) is plotted against the alkyl chain carbon number (Figure 1), a rough estimate of the inorganic wall thickness can be obtained by extrapolation to $n = 0$.[18] This gives an intercept of 28.2 Å and a slope of 0.5 Å per C atom. The slope indicates that the surfactant molecules are stacked in a monolayer tilted against the normal vector of the layers. For comparison, in the case of an untilted monolayer, one would expect a slope of around 1.26 Å per C atom (C−C distance) and in the case of an untilted bilayer 2.56 Å per C atom. The inorganic wall thickness of around 28 Å is significantly larger than those reported previously[18] using a similar synthetic method. Namely, in the latter study the smaller values of 16 Å ($n = 10$, 12, 14) and 11 Å ($n = 16$, 18) were obtained, respectively.[18] In marked contrast, our results show a steadily increasing d_{001} spacing with surfactant chain length and, in agreement with this finding, a nearly constant Fe:surfactant ratio in the final composites (Table 1). Taking an average Fe···Fe distance of 3 Å, these ratios lead to an estimated inorganic wall thickness of 30 Å, which is thus in reasonable agreement with the value of 28 Å determined by the extrapolation of the d_{001} spacings against the alkyl chain carbon number. On the basis of the relative intensities of the second-order diffraction peaks for samples with $n = 16$

(20) Ressler, T. *J. Synchrotron Rad.* **1998**, *5*, 118.
(21) Mustre, J.; Yacoby, Y.; Stern, E. A.; Rehr, J. J. *Phys. Rev. B* **1990**, *42*, 10843.
(22) Rehr, J. J.; Mustre de Leon, J.; Zabinsky, S. I.; Albers, R. C. *J. Am. Chem. Soc.* **1991**, *113*, 5135.
(23) Mustre de Leon, J.; Rehr, J. J.; Zabinsky, S. I.; Albers, R. C. *Phys. Rev. B* **1991**, *44*, 4146.

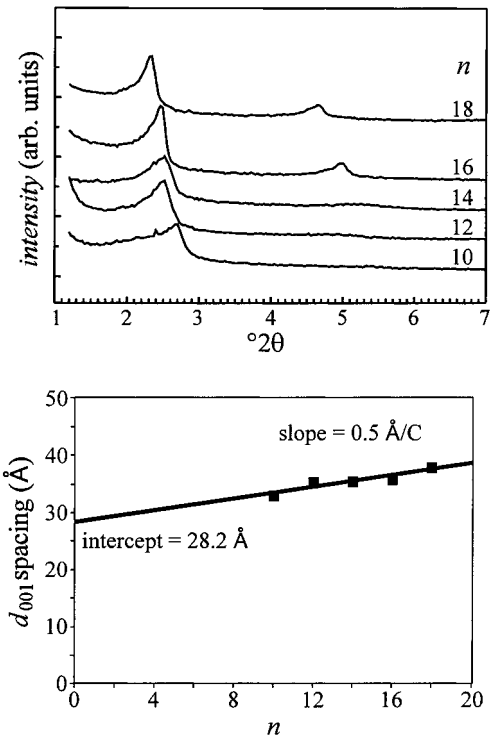

Figure 1. Top: Powder XRD patterns of samples obtained by oxidizing an Fe(II) solution in the presence of C*n*. Bottom: Straight line extrapolation of d_{001} spacing to zero number. The intercept corresponds to the inorganic wall thickness (for the slope, see text).

Table 1. d_{001} Spacings, Compositions, and Average Inorganic Wall Thickness for Iron Oxyhydroxide−Surfactant Composites

n	C*n*/H_2O_2	C*n*/NH_3 (pH = 1.90)	C*n*/NH_3 (pH = 2.00)	C*n*/NH_3 (pH = 2.13)
10	33.0	39.0*	42.0	41.6
12	35.2	42.0	43.2	45.7[a]
14	35.4	48.8	47.4	49.0
16	35.8	50.7	49.5	52.3
18	37.8	54.5	53.1	55.3
Fe:2 surfactant (average molar ratio)	9.8:2.0	6.5:2.0	7.8:2.0	10.2:2.0
slope (Å/#C)	0.5	2.0	1.6	1.6
inorganic wall thickness (Å)	28.2	19.2	24.5	26.4

[a] Value excluded for the determination of the inorganic wall thickness and average composition because the composition of this compound deviates significantly from the average value for this series.

and $n = 18$, the long-range order of those lamellar composites is more regular.

TEM images (Figure 2) reveal that the mesocomposites have a spherical morphology with an average diameter of only around 100 nm. Higher resolution images underline the lamellar nature of these compounds and hence confirm the conclusions drawn from XRD measurements. The d_{001} spacing of 37 Å obtained from TEM for the compound with C12/H_2O_2 is in reasonable agreement with the value from XRD measurements (35.2 Å).

Experiments carried out under the same reaction conditions, but with a very rapid addition of the H_2O_2 solution (within 10 s), show XRD patterns, which in addition to the d_{001} reflections exhibit broad features at around 0.8°−1.2° 2θ. For this reason, these samples

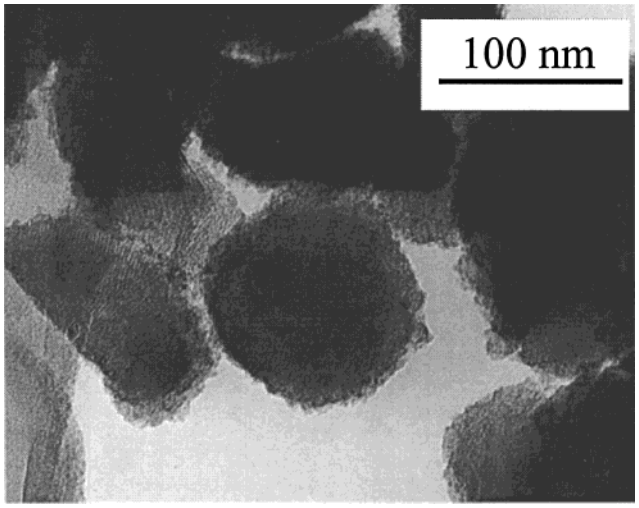

Figure 2. TEM image of iron oxyhydroxide−surfactant composites obtained by oxidizing an Fe(II) solution with H_2O_2 in the presence of C12.

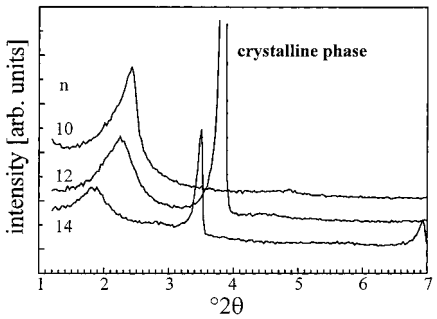

Figure 3. XRD patterns showing the presence of a crystalline phase and mesocomposites for samples prepared by hydrolysis of an Fe(III) solution with NH_3 addition (pH = 1.85).

were not investigated in detail; an analysis of their d_{001} spacings gives an average inorganic wall thickness of 32 Å, demonstrating that the faster addition of H_2O_2 results in a slightly increased thickness of the inorganic part.

When the second method, that is, addition of NH_3, is used to promote the hydrolysis of Fe(III), a precipitation of similar layered composites can also be achieved. Here, NH_3 is added to an Fe(III) solution and after a certain aging time the surfactant solution is added. Four series of compounds were prepared by varying the amount of NH_3 added. In the first series, the starting pH was adjusted to 1.85. The addition of a base forces the hydrolysis, but in this series the pH increase is too small to promote a reaction leading exclusively to composites with relatively thick inorganic walls. Instead, as shown in Figure 3, for longer alkyl chain surfactants the XRD patterns indicate the presence of crystalline phases, which have been previously described in ref 18 together with products similar to those obtained by H_2O_2 oxidation (thick inorganic walls). The crystalline phases also exhibit sharp high-angle reflections. Only for C10, the product is a phase pure lamellar composite with thick inorganic walls. Obviously, the alkyl chain length and hence the van der Waals interactions between the surfactant alkyl chains play a significant role in determining the product, a fact which will be discussed below.

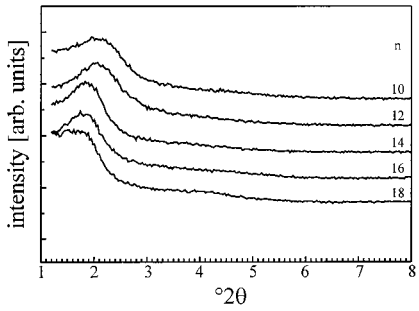

Figure 4. Typical XRD patterns for C*n*/NH_3 samples (pH_{start} = 2.0).

When the pH is further increased, the formation of crystalline phases is completely suppressed and only mesolamellar composites are obtained. Typical XRD patterns are shown in Figure 4 for a starting pH of 2.0. In contrast to samples prepared by oxidation, only d_{001} reflections are detected. In addition, these reflections are relatively broad, indicating that these materials are not as well ordered as the composites obtained by oxidation. When the extrapolation of d_{001} spacings is used again against zero carbon number (Table 1), together with elemental analysis, the advantage of the NH_3 method for controlling the inorganic wall thickness becomes clearly visible: The thickness of the inorganic walls increases with increasing pH because the addition of a base forces hydrolysis of the Fe(III) species and initiates the growth of the polymeric inorganic precursors. In the final step, exactly after 2 h, the addition of a surfactant results in the coordination of the latter to the precursor ions through strong electrostatic interactions and leads to the formation of the inorganic/organic array. The fit results (Table 1) confirm that the hydrolysis forced by NH_3 gives mesocomposites with freely adjustable (between 19 and 27 Å) inorganic wall thicknesses with increasing pH. Hence, by carefully choosing the synthesis conditions, the thickness of the inorganic part can be finely tuned, depending upon the amount of base added.

The morphology of these composites is quite different from those prepared by H_2O_2 oxidation. In contrast to the latter, in which particles are highly agglomerated, but can be differentiated by TEM inspection, the solid consists in this case of larger particles having smooth surfaces with dimensions up to 200 μm (Figure 5), constituted from small, single particles.

In a modification of this reaction, the precursor solutions were aged for different times. This results in larger inorganic precursors that self-assemble with the organic surfactants after the addition of the latter.[19] The evolution of the d_{001} spacing with increasing aging time is depicted in Figure 6 for C12. Clearly, as a result of prolonged aging times, the contribution of the larger precursors to the layer thickness increases. This is also corroborated by an increase of the Fe content in the final composites.[24]

Local Structure of the Inorganic Wall. X-ray absorption spectroscopy is a valuable tool for the characterization of the local structure of iron oxides and has been applied to both crystalline and highly disordered iron oxyhydroxide compounds. Especially in the latter case, structure determination by EXAFS in combination with the simulation of XRD patterns (which generally exhibit only few broad reflections) can be applied to yield information about the poorly ordered structures of, for example, ferrihydrite and feroxyhite.[25−27]

Generally, in the case of pure octahedral coordination, "[FeO_6]" units (Fe coordinated by O^{2-}, OH^-, and H_2O ligands) may be linked by corners, edges, or faces (Figure 7).[25] The Fe···Fe distances depend on the type of linkage and are characteristic of the different types of connection (see Figure 7). Edge-sharing octahedra result in Fe···Fe distances of around 3.0−3.34 Å whereas connection via corners increases the Fe···Fe distance to at least 3.39 Å. On the other hand, face sharing brings the iron ions closer together and shortens the Fe···Fe distance (e.g., to 2.89 Å in hematite).

These different topologies can be discriminated by their radial distribution functions around the Fe ions, which can be obtained from Fe K edge EXAFS spectra and which are directly correlated with both the coordination numbers and the next and next nearest neighbor distances of an Fe^{3+} ion. This makes this type of spectroscopy a sensitive method to probe the (average) local structure of iron oxyhydroxides and similar transition metal compounds.[28,29] Radial distribution functions can thus be used to differentiate between various phases. However, if the distance difference between the atoms constituting particular coordination shells are too small, not all distances can be resolved by EXAFS, even for structurally well-characterized compounds. In such cases the resolution is limited to around 0.10 Å. In this respect, a consideration of the Debye−Waller factors σ is of interest because static disorder, that is, a distribution of interatomic distances, increases the σ values and hints toward a possible contribution of two or more subshells. Satisfying and correct fits can then be obtained both by assuming a single shell with a broad Gaussian distribution of distances or a two-shell model with relatively narrow distance distributions.[25]

XANES (X-ray Absorption Near-Edge Spectroscopy). In the XANES region, pre-edge peaks are detected for all composites at around 7.114 keV (Figure 8). These peaks are assigned to transitions from the 1s level to 3d-like states.[30] Formally, they are dipole-forbidden for perfect octahedral coordination. In all iron oxyhydroxides, however, the coordination deviates from ideal O_h symmetry, resulting in weak pre-edge peaks. In detail, these peaks correspond to electronic transitions to t_{2g} and e_g states arising from the crystal field splitting. The values for the mesocomposites give splittings of around 1.4 eV. These values are slightly smaller than the value of 1.7 eV obtained from optical spectroscopy and theoretical calculations performed for an $[FeO_6]^{9-}$ cluster,[30] but they are in excellent agreement with those of bulk iron oxyhydroxides.

(24) With increased aging time the Fe: 2C12 ratio increases continually from 5.9:2.0 (50 min) to 6.6:2.0 (1500 min).

(25) Manceau, A.; Drits, V. A. *Clay Miner.* **1993**, *28*, 165.
(26) Drits, V. A.; Sakharov, B. A.; Salyn, A. L.; Manceau, A. *Clay Miner.* **1993**, *28*, 185.
(27) Drits, V. A.; Sakharov, B. A.; Manceau, A. *Clay Miner.* **1993**, *28*, 209.
(28) Manceau, A.; Combes, J. M. *Phys. Chem. Miner.* **1988**, *15*, 282.
(29) Manceau, A.; Gorshkov, A. I.; Drits, V. A. *Am. Miner.* **1992**, *77*, 1144.
(30) Sherman, D. M.; Waite, T. D. *Am. Miner.* **1985**, *70*, 1262.

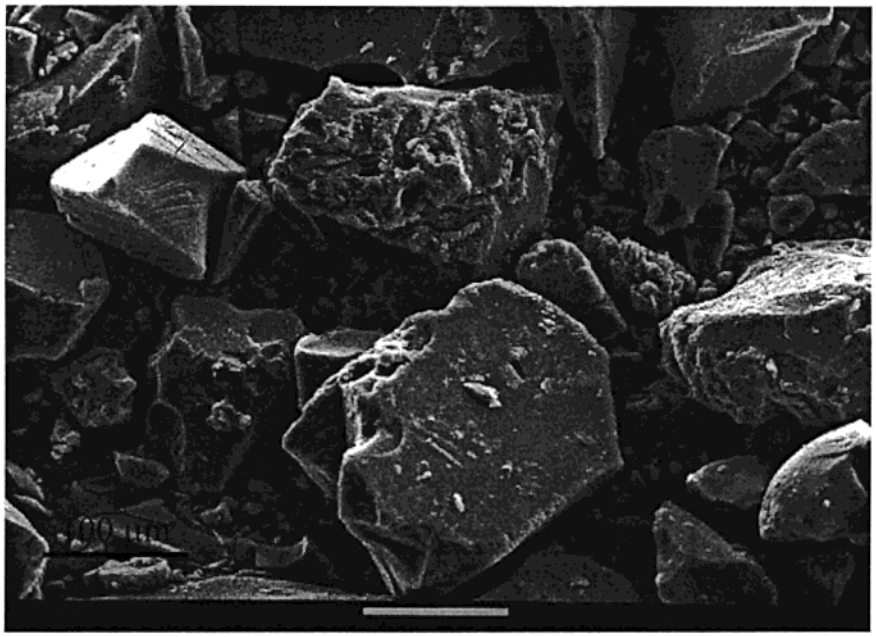

Figure 5. Representative SEM image of a sample prepared by hydrolysis with NH_3.

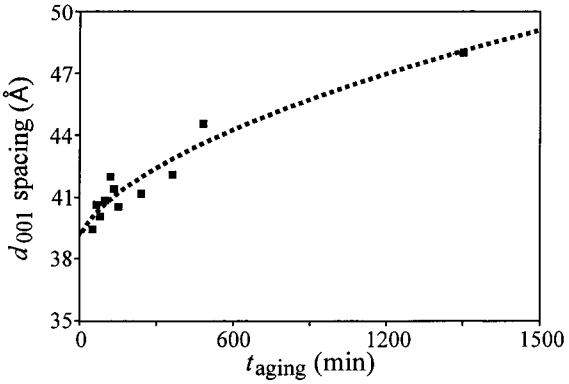

Figure 6. Plot of d_{001} spacings against the aging time showing the increase in the layer spacing with aging time for C12/NH_3.

Above the edge, the absorption curves of the composites are relatively unstructured compared to bulk crystalline oxides (Figure 8). This also holds for the precursors occurring during the first stages of iron oxide formation.[31,32] Although it is clear that no quantitative picture can be derived from XANES, the spectra show that the average short-range order and composition within the inorganic part of the mesocomposites is similar to those of bulk iron oxyhydroxides rather than to iron oxides.

EXAFS. The FTs of the Fe K EXAFS spectra of the C*n*/H_2O_2 samples are shown in Figure 9. Back-transformation of the first peaks of each FT gives isolated EXAFS functions. Fits to these functions, depicted for two C*n*/H_2O_2 samples with a short and a long alkyl chain surfactant in Figure 10, yield average Fe−O distances of 2.07(1) Å for the first coordination shell (Table 2). Such values are usually found for octahedral coordination in bulk iron oxyhydroxides. The large values of σ^2 and also of the higher order cumulants C_3 and C_4 (Table 2) indicate that the oxygen environments around the iron ions are strongly disordered in these samples.

For the second and third shells corresponding to Fe···Fe distances, values of 3.02−3.07 and 3.38−3.43 Å were evaluated (Table 3). Representative fits are also shown in Figure 10. These distances are attributed to octahedrally coordinated iron ions, which are interlinked by common edges (around 3.04 Å) and corners (around 3.40 Å). A comparison with bulk iron oxyhydroxides and oxides shows that these distances are close to those found for goethite and akaganéite. EXAFS analysis thus reveals that the *average* local structure around the Fe ions is similar to those of the mentioned bulk iron oxyhydroxides. The σ^2 values for the second shell are relatively high, which can be either due to a contribution of other kinds of linkages, for example, face-sharing, or to a relatively large disorder.[25] On the basis of the fact that fits including an additional peak at around 2.9 Å gave very low coordination numbers of typically 0.2, the first possibility can be excluded and the large σ^2 values must be explained in terms of structural disorder around the next-nearest Fe coordination shell. This is supported by the low coordination numbers found, which evidence that many vacancies are present, as was also found for less-crystalline iron oxyhydroxides such as feroxyhite.[25] For C12/H_2O_2, the EXAFS exhibits a wave beating around 11 $Å^{-1}$, which indicates the existence of an akaganéite-like part in the local structure and points to the presence of two subshells arising from different Fe···Fe distances differing by 0.14 Å. On the other hand, the fact that no wave-beating is detected for C16/H_2O_2 clearly indicates that the rapid oxidation with H_2O_2 at higher temperatures can lead to mesocomposites with a slightly different average local structure and an increased linkage between the individual $\{Fe[O^{2-}_x, (OH^-)_y, (OH_2)_z]_{x+y+z=6}\}$-units.

When the low coordination numbers found are considered, the contribution of surface ions has to be taken into account in addition to the possibilities of Fe vacancies occurring in a perfect two-dimensional or-

(31) Combes, J. M.; Manceau, A.; Calas, G.; Bottero, J. Y. *Geochim. Cosmochim. Acta* **1989**, 53, 583.
(32) Combes, J. M.; Manceau, A.; Calas, G. *Geochim. Cosmochim. Acta* **1990**, *54*, 1083.

Fe ··· Fe distances (Å)		face	edge	corner
goethite	(α-FeOOH)		2× 3.01, 2× 3.28	4× 3.46
akaganeite	(β-FeOOH)		2× 3.03, 2× 3.34	4× 3.51
lepidocrocite	(γ-FeOOH)		6× 3.06	2× 3.87
feroxyhite	(δ'-FeOOH)	2.88	2.95-3.18	3.39
hematite	(α-Fe_2O_3)	1× 2.89	3× 2.97	3× 3.39, 6× 3.70

Figure 7. Possible linkages of octahedra in Fe(III) oxides and oxyhydroxides and corresponding Fe···Fe distances for some bulk iron oxyhydroxides.

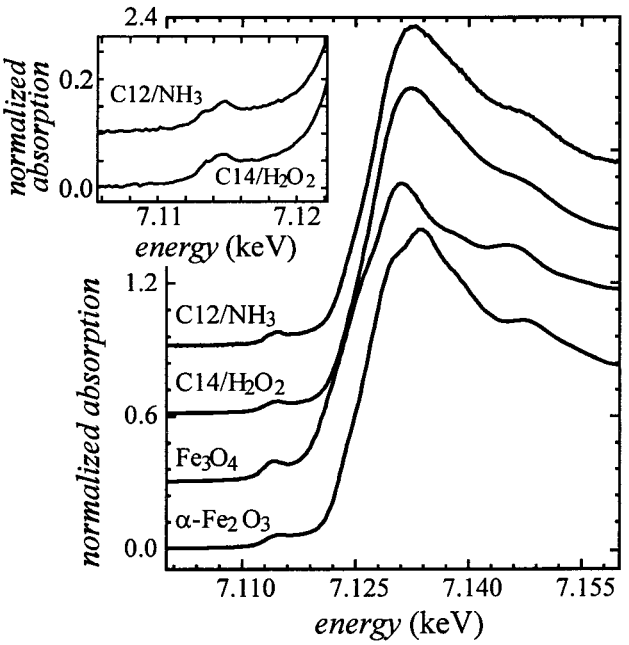

Figure 8. Fe K XANES spectra of iron oxyhydroxide–surfactant composites prepared by different methods in comparison to those of Fe_3O_4 and α-Fe_2O_3. Spectra are offset for clarity. The inset shows the pre-edge transition of the two top spectra in detail.

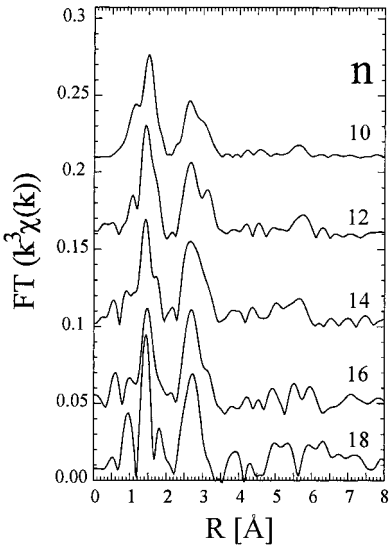

Figure 9. Representative k^3 weighted FTs of C*n*/H_2O_2 samples (spectra are offset for clarity).

dered inorganic array and in addition to structural disorder. On the basis of the composition obtained by elemental analysis (Fe: 2 surfactant molecules = 9.8: 2.0, Table 1), ≈20% of the iron ions can in principle coordinate to surfactant ions[33] and hence have a reduced number of next-nearest Fe neighbors. In addition, given the possibility that the inorganic part consists of partly linked clusters instead of a perfect two-dimensional array, a further decrease of the average Fe···Fe coordination number can be expected.

Typical FTs of samples prepared by NH_3 addition are depicted in Figure 11. EXAFS analysis (Figure 12) of the first coordination shell gives Fe–O distances of 2.06–2.08 Å, again indicative of an octahedral oxygen coordination (Table 4). As for the C*n*/H_2O_2 samples, the large values of the higher order cumulants show that the local environments of the oxygen shell around the iron ions are highly disordered. This is similar to X-ray absorption studies on the formation of bulk iron oxides, where polymers and less-ordered oxyhydroxides were shown to occur at the first stages of precipitation.[31,32]

Compared to the materials prepared by the H_2O_2 route, fits (Figure 12) obtained for the second and the third shell for the NH_3 route gave higher coordination numbers. The fit results for the second and the third shell, collected in Table 5, reveal that the average coordination number slightly increases with higher starting pH values, that is, with the amount of base added. A higher starting pH value results in increased linking between the [FeO_6] units. In comparison with the H_2O_2 samples, the second shell Fe···Fe coordination numbers for C12/NH_3 compounds are distinctly higher, a fact that can be attributed again to the longer aging time: In the case of the H_2O_2 method, the relatively rapid oxidation results in solid mesocomposites precipitated by the surfactants within minutes. This shortens the time available for condensation within the inorganic part and manifests itself in lower coordination numbers.

Summarizing the results of the EXAFS analyses, we conclude that, despite certain differences, both preparative methods lead to composites with nanometer-sized iron oxyhydroxides having an *average* local structure reminding of those found for the bulk iron oxyhydroxides goethite and akaganéite.

(33) This is supported by the fact that the vibrations in the IR spectra of the $-OSO_3$ group are shifted in comparison with those of the free surfactant.

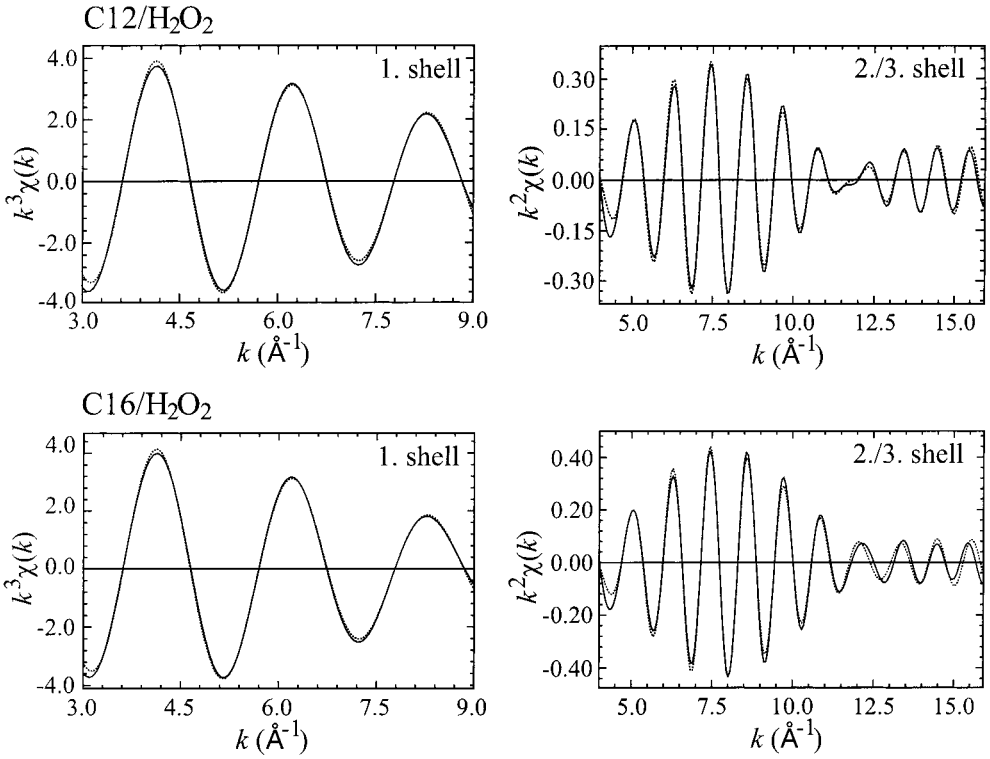

Figure 10. EXAFS fits (dotted) to the back-transformations (full lines) of the first peak (left side) and the second and third (right side). The data correspond to the FTs given in Figure 9.

Table 2. Fit Results for the Back-transformed First Peak of C*n*/H_2O_2 Samples (k = 3−9 Å^{-1}, Weighted with k^3)[a]

n	R (Å)	CN	ΔE (eV)	$\sigma \times 10^3$ (Å^2)	$C_3 \times 10^3$ (Å^3)	$C_4 \times 10^4$ (Å^4)
10	2.07	6.69	3.79	1.75	1.3	3.4
12	2.07	6.09	2.60	1.23	1.5	1.9
14	2.06	6.69	3.17	1.67	1.4	3.2
16	2.08	6.60	2.89	1.21	1.7	1.0

[a] CN denotes coordination number, σ^2 the Debye−Waller factor, and C_3 and C_4 the higher order cumulants, respectively. S_0^2 was fixed to 0.7. Fe−O distances are accurate to ±0.02 Å.

Table 3. Fit Results of EXAFS Analysis of the Second/Third Coordination Shell for C*n*/H_2O_2 Samples (k = 4−16 Å^{-1}, Weighted with k^2)[a]

	second shell				third shell			
n	CN	R (Å)	$\sigma^2 \times 10^3$ (Å^2)	ΔE_0 (eV)	CN	R (Å)	$\sigma^2 \times 10^3$ (Å^2)	ΔE_0 (eV)
10	1.6	3.04	6.4	−1.0	0.6	3.42	3.2	−1.0
12	1.6	3.03	4.1	−2.6	0.6	3.43	0.1	−2.6
16	1.8	3.02	3.2	−3.9	0.9	3.40	2.5	−3.9

[a] CN denotes coordination number, σ^2 the Debye−Waller factor. S_0^2 was fixed to 0.7 and Fe···Fe distances are accurate to ±0.02 Å.

We also checked XRD patterns for high-angle reflections to get information about a possible crystalline structure within the inorganic part. Indeed, experiments with Cu Kα radiation showed broad and weak reflections, not attributable to any particular single bulk phase. As iron strongly absorbs Cu Kα radiation, we also checked the same samples with Cr Kα radiation, but no reflections were detected. Thus, the broad reflections in the former case can be assigned to arise from restructuring during the measurements, possibly induced by local heating. Generally, the mesocomposites do not give rise to high-angle diffraction peaks.

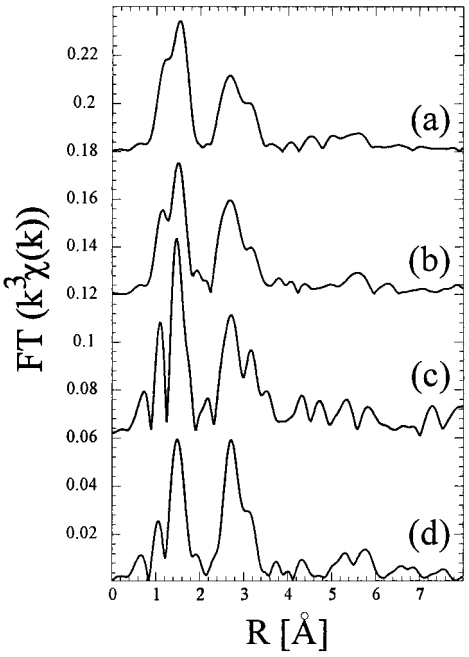

Figure 11. k^3 weighted FTs of C12/NH_3. (a) pH_{start} = 1.90, t_{aging} = 50 min; (b) pH_{start} = 1.90, t_{aging} = 480 min; (c) pH_{start} = 2.00, t_{aging} = 120 min; (d) pH_{start} = 2.13, t_{aging} = 120 min (spectra are offset for clarity).

Magnetic Measurements and Mössbauer Spectra. Typical dc susceptibility measurements for samples prepared by the H_2O_2 method are given in Figure 13. ZFC (zero-field-cooled) curves exhibit a peak, whereas FC (field-cooled) measurements do not, indicative of superparamagnetic behavior. For both compounds in Figure 13, the FC curve does not saturate at low temperatures. Hence, at 5 K there are still particles that exhibit independent relaxation. Thus, a cooperative

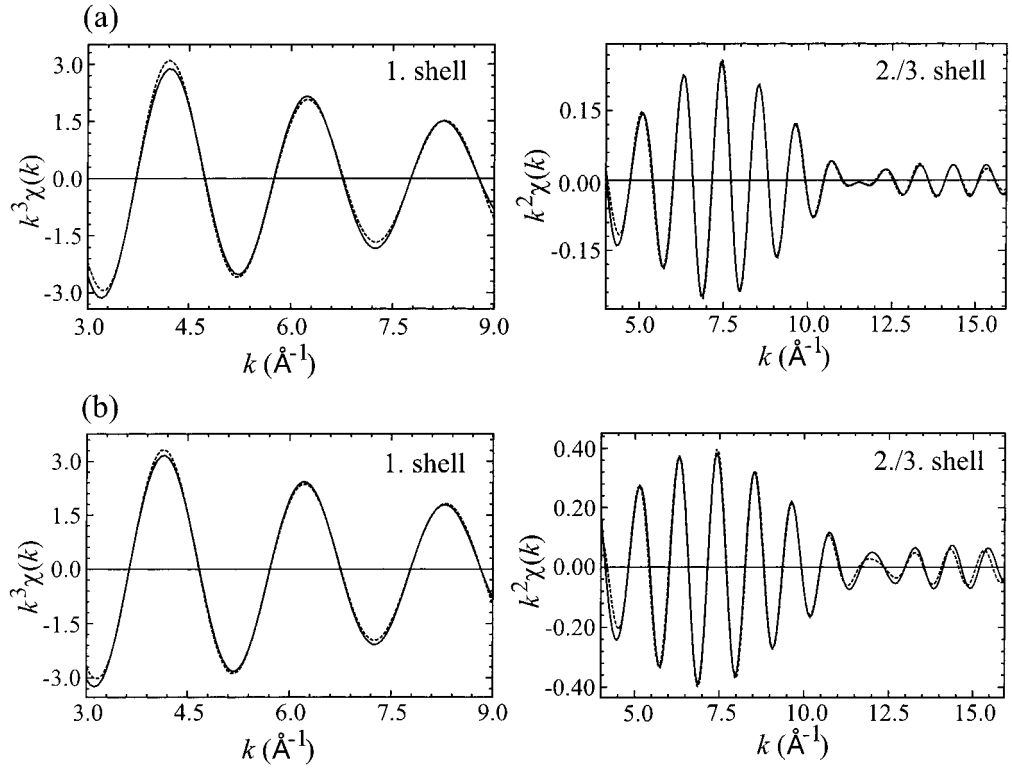

Figure 12. EXAFS fits (dotted) to the back-transformations (full lines) of the first peak and the second and third peak (right side). The back-transformations of (a) correspond to the FT shown in Figure 11a and those of (b) to the FT given in Figure 11b.

Table 4. Fit Results for the Back-transformed First Peak C12/NH_3 Samples Obtained at Different Starting pHs and Different Aging Times (k = 3−9 Å^{-1}, Weighted with k^3)[a]

starting pH	aging time (min)	R (Å)	CN	ΔE (eV)	$\sigma \times 10^3$ (Å^2)	$C_3 \times 10^3$ (Å^3)	$C_4 \times 10^4$ (Å^4)
1.90	100	2.06	6.33	4.37	2.18	1.05	4.76
1.90	480	2.06	6.00	3.29	2.32	1.35	5.49
2.00	120	2.08	5.46	3.44	1.41	1.47	3.26
2.13	120	2.07	6.30	3.14	1.93	1.55	4.27

[a] CN denotes coordination number, σ^2 the Debye−Waller factor, and C_3 and C_4 the higher order cumulants, respectively. S_0^2 was fixed to 0.7. Fe−O distances are accurate to ±0.02 Å.

Table 5. Fit Results of EXAFS Analysis of the Second/Third Coordination Shell for Cn/NH_3 Samples (k = 4−16 Å^{-1}, Weighted with k^2)[a]

		second shell				third shell			
starting pH	aging time (min)	CN	R (Å)	$\sigma^2 \times 10^3$ (Å^2)	ΔE_0 (eV)	CN	R (Å)	$\sigma^2 \times 10^3$ (Å^2)	ΔE_0 (eV)
1.90	100	1.9	3.05	8.1	0.4	0.6	3.48	2.7	5.8
1.90	480	1.9	3.04	6.3	−0.6	0.9	3.49	4.7	5.9
2.00	120	2.1	3.06	5.4	1.4	0.4	3.47	1.4	1.4
2.13	120	2.8	3.08	6.5	3.8	0.5	3.47	0.8	4.3

[a] CN denotes coordination number, σ^2 the Debye−Waller factor. S_0^2 was fixed to 0.7 and Fe···Fe distances are accurate to ±0.02 Å.

freezing of the magnetic moments (like in spin glasses) can be excluded.[34] The peak temperatures T_p in the ZFC measurements are 16 and 12 K for the compounds synthesized with C12 and C18, respectively. Former investigations on similar samples for longer alkyl chain surfactant composites showed lower T_p values (below 4 K) in comparison with shorter alkyl chain composites (around 16 K).[18] However, in this investigation the inorganic wall thickness also varied. Here, we have approximately the same inorganic layer thickness for all Cn/H_2O_2 compounds, resulting in similar T_p values.

From ac measurements (between 5 and 1000 Hz, 1100 A m^{-1}) the average magnetic moment per iron ion was determined to 3.4 μ_B by a fit of the inverse susceptibility far above T_p to the Curie law. The low magnetic moment per iron ion implies that the underlying magnetic ordering is antiferromagnetic or antiferromagnetic-like.

Below T_p, magnetization measurements show a small hysteresis, whereas above T_p no hysteresis was detected. Together with the dc/ac susceptibilities measurements, this supports an antiferromagnetic spin alignment within the inorganic part, where the net magnetic moment arises from an imperfect spin alignment and/or uncompensated surface spins. Various possible explanations for the existence of a net magnetic moment have to be taken into account. Vacancies and—in terms of the lamellar nature and the average thickness of the iron oxyhydroxide layer (around 28 Å)—the contribution of iron ions located at the surface and coordinating to the surfactant headgroups (around 20% of the whole inorganic layer) have to be considered. A clear distinction between these two contributing factors is hardly possible because the "surface" ions can also be regarded as entities having vacancies as next-nearest neighbors. Because of the limited size of the inorganic part and the considerable amount of vacancies present (as indicated by the low coordination numbers obtained by EXAFS analysis), most probably both types contribute to the incompleteness of antiferromagnetic ordering. In addition, as was previously shown for feroxyhite, which is a planar antiferromagnet, the presence of an odd

(34) Lázaro, F. J.; García, J. L.; Schünemann, V.; Butzlaff, C.; Larrea, A.; Zaluska-Kotur, M. A. *Phys. Rev. B* **1996**, *53*, 13934.
(35) Bender Koch, C.; Oxborrow, C. A.; Mørup, S.; Madsen, M. B.; Quinn, A. J.; Coey, J. M. D. *Phys. Chem. Miner.* **1995**, *22*, 333.

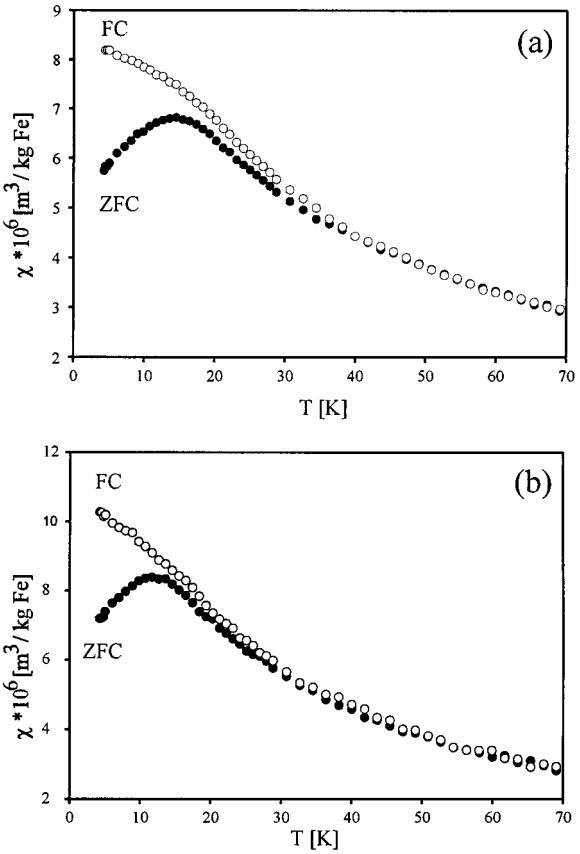

Figure 13. Zero-field-cooled (ZFC) and field-cooled (FC) dc measurements (200 kA m^{-1}) for (a) C12/H_2O_2 and (b) C18/H_2O_2.

number of (octahedral) antiferromagnetic layers results in a nonvanishing net magnetic moment.[35]

In comparison, C*n*/NH_3 compounds gave a quite different appearance in the ZFC/FC measurements. Also for these compounds the magnetic moment of around 3 μ_B obtained in all cases is clearly smaller than 5.9 μ_B (free ion value), thus indicating that again the magnetic ordering is antiferromagnetic. However, as opposed to the former composite materials, the ZFC curves show an unusual temperature dependence for samples prepared at pH 2.0 or above (Figure 14). The ZFC measurements exhibit very broad peaks, which are obviously due to at least two peaks at around 8 and 22 K, respectively. In contrast, the sample prepared at a starting pH of 1.90 exhibits behavior that is dominated by superparamagnetic relaxation down to the lowest measuring temperatures available (around 4 K), and a deviation between the FC and ZFC curves is only visible at temperatures below 6 K. The peak temperatures T_p do not correlate with the d_{001} spacings. The d_{001} values for the samples for which the magnetic measurements are displayed in Figure 14 are 45.4, 43.2, and 45.7 Å, respectively. For compounds with a similar *d* spacing and hence a similar inorganic wall thickness, we would expect similar blocking temperaturees. This is in contrast to the experimental findings (Figure 14). The result can, however, be interpreted in terms of a cluster model. Clusters building up the inorganic part can be smaller than the average inorganic wall thickness and

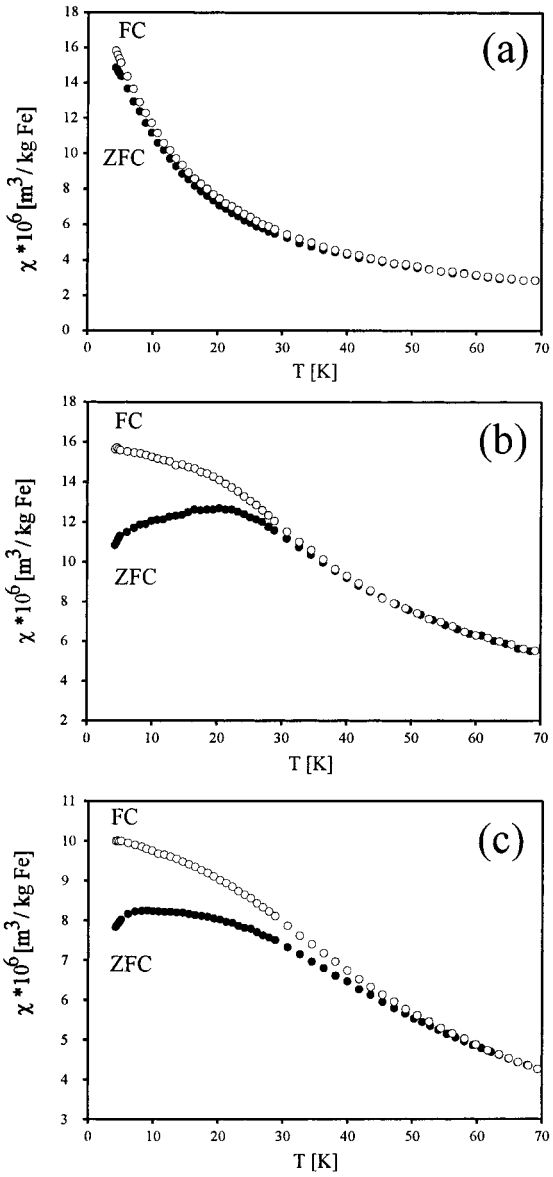

Figure 14. Zero-field-cooled (ZFC) and field-cooled (FC) dc measurements (200 kA m^{-1}) for C12/NH_3 compounds. (a) $pH_{start} = 1.90$, $t_{aging} = 480$ min; (b) $pH_{start} = 2.00$, $t_{aging} = 120$ min; (c) $pH_{start} = 2.13$, $t_{aging} = 120$ min.

hence lead to a (broad) distribution of T_p values. This is also supported by XRD, which shows relatively broad d_{001} peaks in comparison with the more ordered H_2O_2-derived samples, evidencing that the variation in layer spacing is larger within a specific C*n*/NH_3 sample. An alternative explanation for the occurrence of the broad peaks in ZFC measurements would be the presence of small-sized bulk iron oxide/oxyhydroxides. From the point of view of the hydrolysis chemistry of iron this cannot be ruled out. However, XRD patterns did not show any peaks in the high 2θ region, so we can rule out the presence of a significant amount of (coprecipitated) bulk materials.

In addition to the investigations described above, Mössbauer spectroscopy was employed. This method is not only suited to derive additional information about the magnetism of these compounds but also acts as a probe for the presence of different parts with varying crystallinity or structure and hence supplements both EXAFS and susceptibility measurements. The Möss-

(36) Matijevic, E.; Sapieszko, R. S.; Melville, J. B. *J. Colloid Interface Sci.* **1975**, *50*, 567.

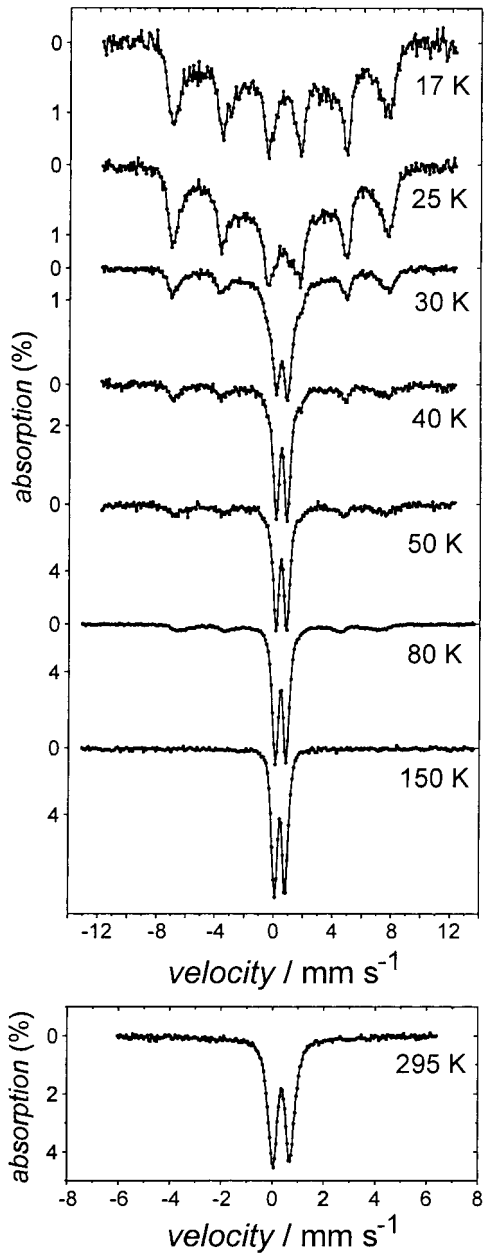

Figure 15. Temperature-dependent Mössbauer spectra of C12/H_2O_2 (note the different scales).

bauer spectra for composites derived by the H_2O_2 route show that more than one component contribute to the spectra. The temperature dependence of the spectra of the C12/H_2O_2 sample is depicted in Figure 15. Despite the fact that the synthesis starts with Fe(II), the Mössbauer parameters indicate that all iron ions in the solid-state structure are present in the form of high-spin Fe(III). The low-temperature spectra are dominated by a sextet, which has the parameters $B_{hf} = 46$ T, $\delta = 0.48$ mm s^{-1}, and $\epsilon = -0.12$ mm s^{-1}. In addition to this sextet, another feature is observed: Down to the lowest measuring temperature a broad component is detected in the centroid of the spectra. At 30 K, this broad feature has become a doublet, which is demonstrated by the flattening of the background close to the centroid of the spectrum. The relative area of the sextet with relatively sharp lines is almost unchanged between 17 and 50 K. This clear difference in the temperature dependence makes it highly probable that these two components, the broad feature and the sharp sextet, stem from different parts; that is, the inorganic part is composed of two phases with different crystallinity. The sharp sextet is attributed to a relatively well-crystallized component. This phase has hyperfine parameters and δ and ϵ values similar to those of goethite, but the hyperfine field B_{hf} is too low compared to that of bulk goethite. This can be explained either by a lower Néel temperature compared to that of goethite (due to the lower dimensionality of the system investigated here) or by the presence of a considerable amount of defects. The latter explanation is supported by EXAFS analysis, which showed the average coordination number of higher shells to be significantly lower than that in the bulk iron oxyhydroxides. The broad sextet, which is almost fully collapsed at 30 K, has a lower value of the hyperfine field (at 17 K about 35 T). Such a low hyperfine field has not been observed for any bulk iron oxide nor oxyhydroxide. In this respect, numerous investigations have focused on the precipitation of iron oxides and oxyhydroxides from chloride, nitrate, and perchlorate salts (e.g., refs 36−41). To summarize, the precipitation of iron oxides/oxyhydroxides is not a spontaneous reaction, but involves the formation of intermediate high-nuclearity iron oxyhydroxide polymers, which then transform into the proper bulk iron oxyhydroxides or oxides upon aging. This process has also been investigated by Mössbauer spectroscopy. Low-temperature spectra (77 K) showed these polymers to have low hyperfine fields of around 42 and 35 T.[42] Moreover, the spectra generally consist of more than one magnetically split component at these temperatures, indicating the presence of different polymeric species. Hence, the close agreement between the low hyperfine values reported for these polymers and for the broad component of C12/H_2O_2 can be taken as evidence for a polymer-like phase within the layers of these mesocomposites prepared by H_2O_2 addition (in addition to the more well-crystalline phase described above). By comparison with the spectra of pure polymers, it is not surprising that two different phases coexist in the solid mesocomposite because the addition of H_2O_2 increases the pH of the solution simultaneously with the oxidation of Fe(II) and thus induces the formation of iron oxyhydroxide polymers:[43]

$$Fe^{2+} + H_2O_2 \rightleftharpoons Fe^{3+} + OH^- + OH^\bullet$$

$$Fe^{2+} + OH^\bullet \rightleftharpoons Fe^{3+} + OH^-$$

Turning to the Mössbauer spectra of C18/H_2O_2, the intensity of the broad component is clearly smaller at 16 K (Figure 16). This indicates a larger effective volume

(37) Murphy, P. J.; Posner, A. M.; Quirk, J. P. *J. Colloid Interface Sci.* **1976**, *56*, 284.
(38) Murphy, P. J.; Posner, A. M.; Quirk, J. P. *J. Colloid Interface Sci.* **1976**, 56, 298.
(39) Murphy, P. J.; Posner, A. M.; Quirk, J. P. *J. Colloid Interface Sci.* **1976**, *56*, 312.
(40) Matijevic, E.; Schreiner, P. *J. Colloid Interface Sci.* **1978**, *63*, 509.
(41) Musiæ, S.; Santana, G. P.; Šmit, G.; Garg, V. K. *Croat. Chem. Acta* **1999**, *72*, 87.
(42) Kauffman, K.; Hazel, F. *J. Colloid Interface Sci.* **1975**, *51*, 422.
(43) Holleman, A. F.; Wiberg, E. V.; Wiberg, N. *Lehrbuch der Anorganischen Chemie*, 101 ed.; de Gruyter: Berlin, 1995.
(44) Flynn, C. M., Jr. *Chem. Rev.* **1994**, *84*, 31.

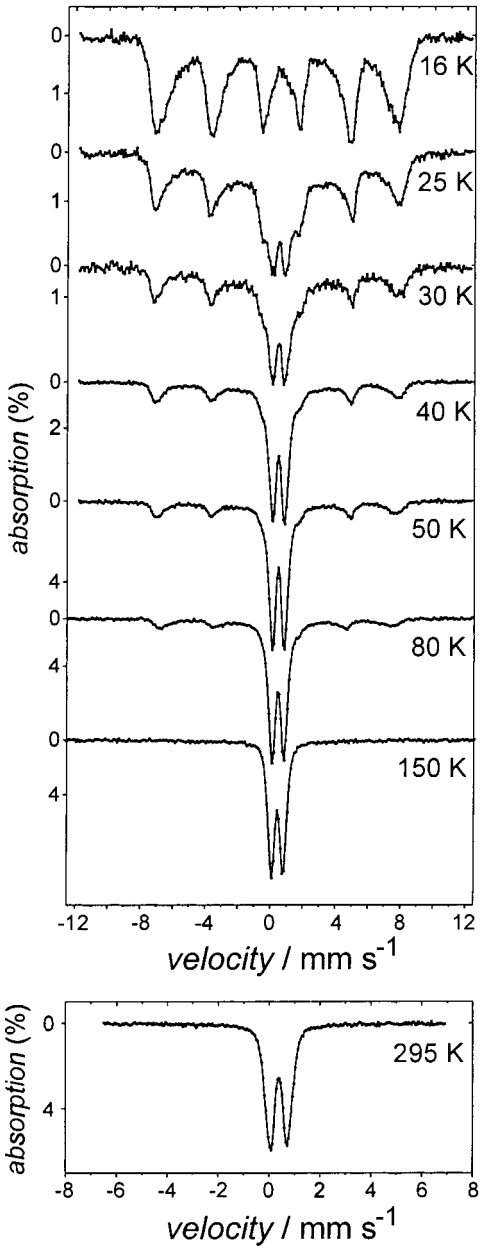

Figure 16. Temperature-dependent Mössbauer spectra of C18/H_2O_2 (note the different scales).

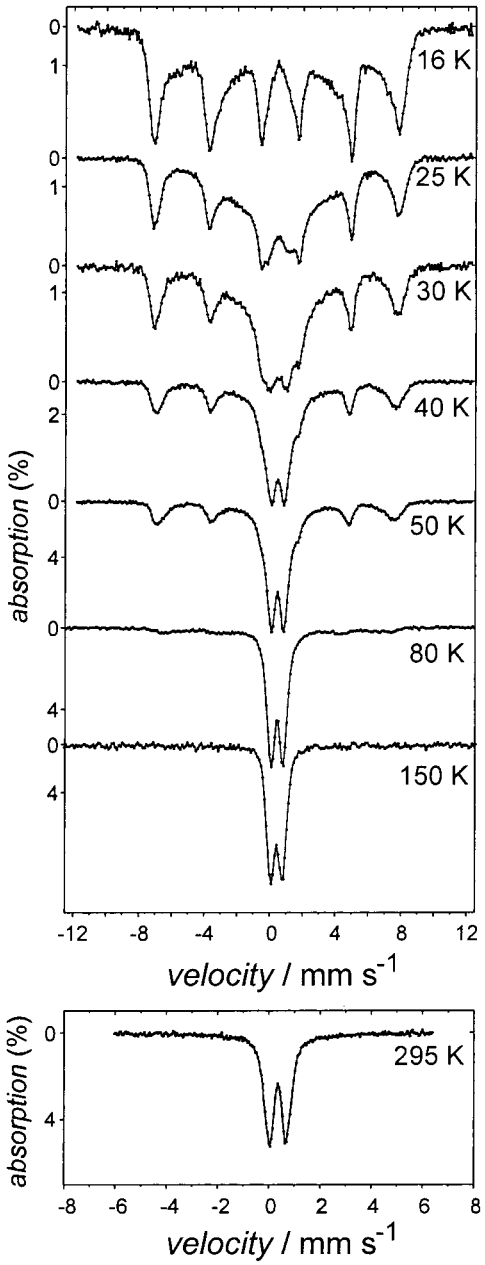

Figure 17. Temperature-dependent Mössbauer spectra of C12/NH_3 (note the different scales).

of the domains. A second sextet is seen as shoulders on lines 1 and 2 and has an estimated hyperfine field at 16 K of about 44 T. We conclude that the spectra of this sample also consist of (at least) two sextets, one which gradually collapses into a doublet over a wide temperature range (as expected for non- or weakly interacting superparamagnetic particles); the other, which is analogous to that found in C12/H_2O_2, changes to a magnetically split doublet within a much smaller temperature region (as observed for interacting particles). Again, the inorganic layers consist of (at least) two parts with different local structures.

Also, for the C12/NH_3 sample, low-temperature spectra show two components: Again, there occur a sharp sextet and a broad one (Figure 17). The Mössbauer parameters (Table 6) of the sharp sextet are similar to those of the sharp sextet observed for C12/H_2O_2, suggesting that these two subphases are identical. This is not surprising, as both methods, the oxidation of Fe(II) with H_2O_2 and the addition of a base to an Fe(III) solution, lead to an increase in pH and thus to a

Table 6. Mössbauer Parameters for Iron Oxyhydroxide−Surfactant Composites (±0.05 for Both δ and ϵ)[a]

compound	T (K)	component	δ (mm s^{-1})	ϵ (mm s^{-1})	B_{hf} (T)
C12/H_2O_2	17	sharp sextet	0.48	−0.13	46
		broad sextet			35*
	295	doublet	0.36	$\Delta E_Q = 0.69$	
C18/H_2O_2	17	sharp sextet	0.48	−0.12	46.4
		2nd sextet			44*
	295	doublet	0.38	$\Delta E_Q = 0.69$	
C12/NH_3	17	sharp sextet	0.48	−0.12	46.6
		2nd sextet			37*
	295	doublet	0.38		
C18/NH_3	16	sharp sextet	0.48	−0.12	47.3
		2nd sextet			46.2
	295	doublet	0.37	$\Delta E_Q = 0.71$	

[a] B_{hf} values are accurate to ±1 T, except those values that are marked with an asterisk (±3 T)

condensation of individual octahedrally coordinated iron ions. In addition, the broad-lined component is similar to the broad component in the corresponding low-temperature spectra of $C12/H_2O_2$, but it collapses to a doublet at higher temperatures and has a more distinct feature at 17 K than that of the $C12/H_2O_2$ sample. This fact may be interpreted in terms of a higher degree of crystallinity of this phase for the sample prepared by aging with NH_3. This is what one would expect because the prolonged aging time (120 min) may result in phases with higher degrees of crystallinity than the relatively short "aging" time of the H_2O_2 method. For the latter route, the "aging time" is determined by the time used for the complete addition of H_2O_2 (generally 150 s), which immediately results in the precipitation of a solid mesocomposite. Thus, the time available for aging and hence to form a more highly ordered phase is much shorter.

The spectra of the $C18/NH_3$ sample are qualitatively different from those of $C12/NH_3$ (Figure 18). At 16 K, the lines are much more narrow because the broad-line sextet is not present. However, as can be seen from close inspection of lines 2, 3, 4, and 6, there is another sextet with relatively sharp lines, which has magnetically split components up to at least 50 K. Similar to $C18/H_2O_2$, the Mössbauer spectra of samples prepared with the longer alkyl chain surfactants indicate different phases. When the spectra of samples synthesized with longer alkyl chain surfactants are compared with those prepared with shorter alkyl chain surfactants, it becomes obvious that these phases, as detected by Mössbauer spectroscopy, are more crystalline, resulting in components with higher hyperfine fields (Table 6). This finding is in good agreement with the EXAFS data, which show the individual $[Fe(O,OH)_6]$ octahedra to be more strongly interlinked for these samples. The main difference in the preparation for short and long alkyl chain surfactants is the slightly higher temperature, which is employed in the syntheses of the longer alkyl chain surfactants (because of their low solubility at room temperature). However, as evidenced by many previous studies on the hydrolysis of Fe(III) salts,[44] a slight temperature increase is sufficient to force the hydrolysis of iron oxyhydroxides, resulting in higher order on a local scale for the samples prepared with longer alkyl chain surfactants.

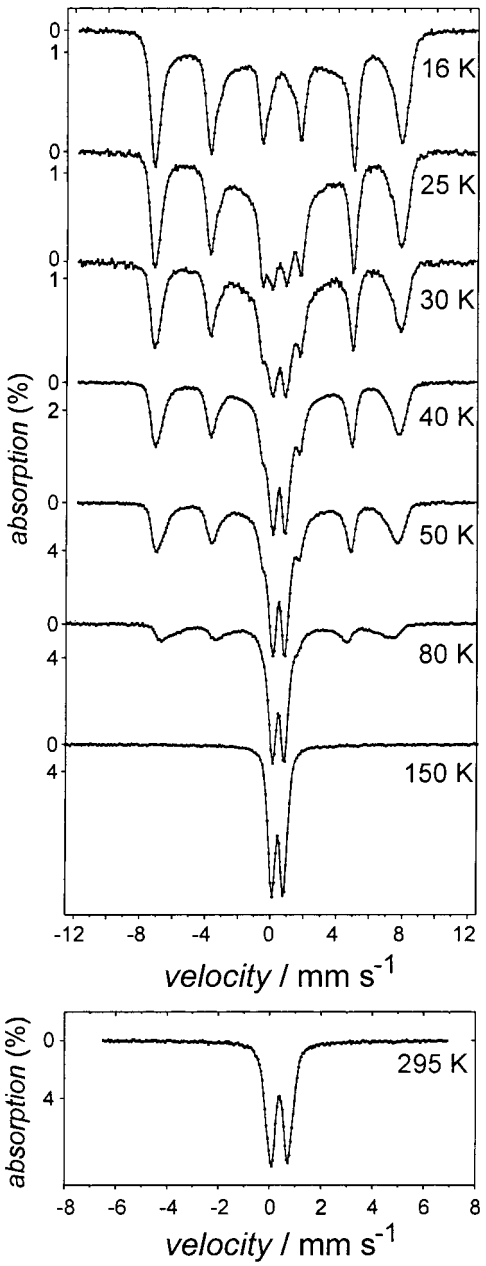

Figure 18. Temperature-dependent Mössbauer spectra of $C18/NH_3$ (note the different scales).

Concluding Remarks

The results discussed here show the possibility of using self-assembly chemistry[45] to synthesize inorganic/organic composites with functional inorganic parts. Simple chemical methods are used to tune the physical properties of the resulting material. Another important point of our study is the diversity of the local structures within the inorganic part that can arise when synthesis parameters are changed slightly, that is, the pH and temperature in this study. On the basis of the results derived from the combined investigation by different spectroscopic techniques, we are also able to suggest synthesis mechanisms for the two different synthesis methods used.

In the samples prepared in our study, the walls are probably built from an array of such clusters. Evidence for this presumption comes from low average coordination numbers for Fe···Fe (EXAFS), the variety of domains with different crystallinity (magnetic measurements and Mössbauer spectroscopy), and the tunability of the inorganic wall thickness. The latter points to a modular construction of the wall rather than to a continuous growth of large oxyhydroxide layers, which would be difficult to control in view of the fast precipitation of the composite. The construction of the inorganic walls of mesostructures from small inorganic clusters is not unusual. In other systems, well-defined polynuclear inorganic precursors such as Keggin ions have been used.[46−48]

(45) Huo, Q.; Margolese, D. I.; Ciesla, U.; Demuth, D.; Feng, P.; Gier, T. E.; Sieger, P.; Firouzi, A.; Chmelka, B. F.; Schüth, F.; Stucky, G. D. *Chem. Mater.* **1994**, *6*, 1176.

(46) Stein, A.; Fendorf, M.; Jarvie, T. P.; Muller, K. T.; Benesi, A. J.; Mallouk, T. E. *Chem. Mater.* **1995**, *7*, 304.

(47) Taguchi, A.; Abe, T.; Iwamoto, M. *Adv. Mater.* **1998**, *10*, 667.

With regard to the organic component of the composites, we note first that negatively charged surfactants such as the ones used here have already been used for inducing the formation of mesostructures of inorganic oxides, starting from salts of the corresponding elements.[46] Especially, dodecyl sulfate C12 was used to form mesostructured oxides of many different compositions.[49−53]

An interesting point to note is the fact that the solution containing surfactants and Fe^{2+} ions does not precipitate a composite with thick inorganic walls. Only upon oxidation of Fe^{2+} to Fe^{3+} coupled with the subsequent growth of ferric oxyhydroxide clusters does a mesolamellar composite form. This is in agreement with a mechanism of mesostructure formation forwarded by Stucky, Schüth, and co-workers,[45] which puts emphasis on the cooperative action of the inorganic and the organic components. This model relies an a chelate coordination between multiply charged inorganic particles offering several coordination sites for the headgroups of the organic surfactants, thus inducing their aggregation. These micelle-like aggregates themselves act as assembly sites for the oxyhydroxide clusters. This theory can also explain the results of syntheses performed according to our second method: Upon addition of NH_3 to an Fe^{3+} solution, ferric oxyhydroxide clusters start to grow. These species do not precipitate within the aging time. With an increasing amount of NH_3 added (increasing pH) and increasing aging time, the clusters grow. Upon addition of the surfactant molecules, these clusters are precipitated to form the inorganic walls of the composite materials. Comparing the two different synthesis methods, it becomes obvious why the "H_2O_2 method" gives materials that possess higher order (as judged by narrower XRD peaks): The oxyhydroxide clusters grow in the presence of the surfactants. When the inorganic particles have reached a certain critical size, they precipitate together with the surfactant molecules. In this way, the size of the precipitated clusters is rather uniform. Applying the "NH_3 method", the clusters grow to a broader distribution of sizes. When the surfactant molecules are then added, they will immediately precipitate all the inorganic clusters, which are larger than a certain critical size.

The fact that samples with an inorganic wall thickness, low average coordination number for Fe···Fe, and the manifold of domains with different crystallinity show that the inorganic wall are most probably built up by a cluster-type array. This may be achieved by the additional incorporation of differently sized precursor clusters into the inorganic wall structure after the reaction is initiated by the surfactant addition and simultaneous cross-linking within the inorganic precursors. The presence of clusters constituting the inorganic wall is not unusual and was found for other systems that start from polynuclear inorganic presursors, for example, Keggin ions.[46−48] The fact that crystalline compounds cannot be obtained with C10 in contrast to mesostructured compounds most probably reflects that not only the cross-linking within the inorganic part but also the van der Waals interaction between the surfactants are important from a thermodynamic point of view.

Supporting Information Available: This material is available free of charge via the Internet at http://pubs.acs.org.

Acknowledgment. This work was sponsored by the Jubiläumsfond der Österreichischen Nationalbank, Grant 7110. We also thank HASYLAB for allocating beamtime and the staff for helpful support during the measurements. A special thanks to H. Schultz, Ludwig-Maximilians-University Munich, for carrying out elemental analysis and Henkel KGaA for supplying surfactants. P.B. acknowledges ongoing financial support from the Fonds der Chemischen Industrie.

CM991211+

(48) Holland, B. T.; Isbester, P. K.; Blanford, C. F.; Munson, E. J.; Stein, A. *J. Am. Chem. Soc.* **1997**, *119*, 6796.
(49) Yada, M.; Hiyoshi, H.; Ohe, K.; Machida, M.; Kijima, T. *Inorg. Chem.* **1997**, *36*, 5565.
(50) Yada, M.; Takenaka, H.; Machida, M.; Kijima, T. *J. Chem. Soc., Dalton Trans.* **1998**, 1547.
(51) Pacheco, G.; Zhao, E.; Garcia, A.; Sklyarov, A.; Fripiat, J. J. *Chem. Commun.* **1997**, 491.
(52) Pacheco, G.; Zhao, E.; Garcia, A.; Sklyarov, A.; Fripiat, J. J. *J. Mater. Chem.* **1998**, *8*, 219.
(53) Ciesla, U.; Demuth, D.; Leon, R.; Petroff, P.; Stucky, G.; Unger, K.; Schüth, F. *Chem. Commun.* **1994**, 1387.